

High-Pressure High-Temperature Synthesis of Hexagonal Boron Nitride Single Crystals from a $\text{Sr}_3\text{B}_2\text{N}_4$ Solvent

Ming Tian,[∇] Ning-Ning Wang,[∇] Gang Wang, Md Al Shahriar Akash, Hui Shi, Junpeng Shu, Ruowang Chen, Nadia Afzal, Zhenning Hu, Shun-Shun Yang, Linglong Zhang, Yu Zhang, Juanjuan Xing, Kenji Watanabe, Takashi Taniguchi, Neng Wan,^{*} and Jinguang Cheng^{*}



Cite This: *Cryst. Growth Des.* 2024, 24, 8557–8562



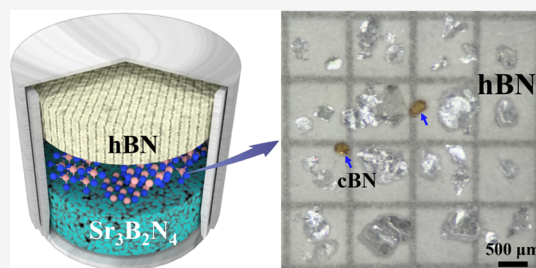
Read Online

ACCESS |

Metrics & More

Article Recommendations

ABSTRACT: We report on high-pressure high-temperature (HPHT) synthesis of high-quality hexagonal boron nitride (hBN) single crystals (SCs) grown out of the novel strontium-based solvent $\text{Sr}_3\text{B}_2\text{N}_4$. Colorless and transparent hBN SCs with lateral sizes up to ~ 1.2 mm were recovered after HPHT synthesis at 4.5 GPa and 1500 °C. The quality of the obtained hBN SCs was characterized using X-ray diffraction (XRD), Raman spectroscopy, cathodoluminescence (CL), and X-ray photoelectron spectroscopy (XPS). The narrow peaks observed in both the XRD and Raman spectra indicate excellent crystalline quality for the hBN SCs. Intense CL peaks centered around 5.76 eV were detected in the hBN SCs grown from high-purity precursors. Additionally, the low residual oxygen level in the hBN precursor powder was identified as a critical factor for achieving a high yield of hBN SCs. We also verified the viability of this route in both a Kawai-type two-state multianvil apparatus with a small-sized chamber and a cubic anvil apparatus with a large-sized chamber. Our work demonstrates that the strontium-based $\text{Sr}_3\text{B}_2\text{N}_4$ solvent provides a low-cost alternative for growing high-quality hBN SCs under HPHT conditions.



1. INTRODUCTION

Hexagonal boron nitride (hBN) is an ultrawide band gap (~ 5.95 eV)¹ III–V group semiconductor with a layered structure akin to graphite. Because of its outstanding properties, such as chemical inertness² and atomically smooth surface³ without dangling bonds, hBN has been widely utilized as an excellent substrate and protection layer for 2D materials.^{4,5} In addition, hBN has been envisioned as a promising candidate for deep ultraviolet (DUV) light-emitting devices due to its high quantum yield.^{6,7} It is also suitable for high-performance solar-blind detectors because of its high selectivity in the solar-blind wavelength region.⁸ Moreover, as a natural hyperbolic material possessing high confinement and low loss of phonon polaritons,⁹ hBN is a promising choice for hyperlenses.¹⁰ All these aforementioned applications require high-quality hBN single crystals (SCs), which are no longer attainable through alternative methods such as chemical vapor deposition,¹¹ sputter deposition,¹² or molecular beam epitaxy.¹³

The methods for growing bulk hBN SCs can be divided into three categories. The first involves polymer-derived hBN crystals with lateral sizes exceeding a few millimeters, using B–N-containing polymers combined with a sintering process.¹⁴ Such hBN SCs exhibit high quality, as evidenced by narrow full width at half maximum (fwhm) in the Raman spectrum. The other route involves growth under ambient pressure and high

temperature (APHT) conditions using metal fluxes such as Ni–Mo,¹⁵ Ni–Cr,¹⁶ Co–Cr,¹⁷ Fe–Cr,¹⁸ or Cu–Cr.¹⁹ This method can yield large crystals with lengths up to several millimeters and thicknesses reaching several hundred microns. The third route entails growing hBN SCs from solvents (or precursors) containing Na,²⁰ Mg,²¹ Ba,²² or Ni²³ under high-pressure high-temperature (HPHT) conditions of 2.5–6 GPa and 1300–2100 °C. So far, Mg²¹- and Ba-based²² solvents have proven to be the most successful precursors for obtaining bulk hBN SCs up to ~ 2 mm in size, with high purity and low defect density. These merits enable HPHT crystals to be widely used in the community of 2D materials. However, HPHT growth requires meticulous control over both the precursors and the growth parameters. Typically, Ba- or Na-based solvents are hygroscopic and prone to rapid oxidation when exposed to air. In addition, the commonly used Ba-based precursor, barium nitride (Ba_2N_3), has a relatively high price (~ 86 USD/gram for typical purity 99.9%). In comparison, Mg-based precursors are more stable and cost-effective.

Received: August 1, 2024

Revised: September 26, 2024

Accepted: September 26, 2024

Published: October 4, 2024



However, the magnesium element tends to produce p-type doping,²⁴ which might induce negative effects on the hBN properties especially when it is used as an insulator. Additionally, the Ni-based system generally produces tiny SCs ranging from 10 to 25 μm . Therefore, it is highly desirable to find a stable and inexpensive solvent system that can yield large, high-quality hBN SCs.

In this study, we demonstrate that a strontium (Sr)-based precursor serves as a cost-effective solvent system for growing high-quality hBN SCs. Compared to the Ba-based system, the Sr-based system is significantly more affordable (Sr_3N_2 , ~ 4.1 USD/gram for purity $\sim 99.9\%$). The high quality of the as-synthesized hBN SCs was confirmed through a suite of analytical techniques, including X-ray diffraction (XRD), Raman spectroscopy, cathodoluminescence (CL), and X-ray photoelectron spectroscopy (XPS).

2. EXPERIMENTAL DETAILS

2.1. Preparation. To remove residual oxygen and other volatile contaminants, the hBN powder (Saint-Gobain Co Ltd., type SP-6, confirmed by XRD to be of the typical hBN phase) was heat-treated at 2000–2100 $^\circ\text{C}$ for 2–6 h in flowing nitrogen gas. The oxygen content of the BN source was measured before and after heat treatment, showing values of approximately 0.66 and 0.09 wt %, respectively, using an oxygen nitrogen analyzer (YANRUI Co Ltd., type ON-330). In this study, we utilized both the heat-treated and the untreated hBN powders for SC growth.

A solvent with the composition of $\text{Sr}_3\text{B}_2\text{N}_4$ was synthesized by sintering a mixture of strontium nitride (Sr_3N_2) powder and high-temperature heat treatment hBN powder (1:2 molar ratio) at 1050 $^\circ\text{C}$ for 12–24 h in a tube furnace. To eliminate residual air in the tube, the tube was evacuated 3–5 times using dry nitrogen flow before sintering, while the dry nitrogen atmosphere was applied during the entire sintering process with a flow rate of 200 sccm. After sintering, the solvent was immediately transferred and stored in an argon-filled glovebox with the H_2O and O_2 concentrations below 5 ppm.

The HPHT synthesis of hBN SCs was initially performed using a Kawai-type two-state multianvil apparatus (Mavo press LPRU 2000–650/150, Germany) with a small chamber size, and it was later scaled up using a modified large-chamber cubic anvil apparatus (Zheng Zhou SANMO Co., Ltd.). No distinct differences were observed in the hBN SCs produced by the small or large chamber apparatus; therefore the results below are reported without specific reference to the dedicated HPHT apparatus, unless otherwise noted.

For the HPHT growth in the cubic anvil apparatus, the $\text{Sr}_3\text{B}_2\text{N}_4$ solvent and hBN powder were encapsulated in a 5.5 mm diameter cylindrical molybdenum (Mo) capsule at a mass ratio of 4:1, which was then placed inside a pyrophyllite cube with a graphite heater, as shown in Figure 2b. The assembling of the HPHT cells was conducted inside the glovebox. After HPHT synthesis, the hBN SCs were recovered by dissolving the Mo capsule in aqua regia.

2.2. Characterizations. XRD was performed on a Rigaku Smartlab X-ray diffractometer with $\text{Cu-K}\alpha$ radiation at room temperature with a scanning range of 20–90 $^\circ$ and a scanning speed at 10 $^\circ$ /min. Raman spectra were carried out at room temperature using a MonoVista CRS+ 500, Spectroscopy and Imaging GmbH or Spectrapro HRS-500 Raman microscope system. A 532 nm laser with power below 1 mW was used, focused to a spot size of approximately 0.72 μm using a 100 \times lens (NA = 0.9). By using a 1200 grooves/mm grating, we achieved a spectral resolution of ~ 0.4 cm^{-1} . All Raman spectra were calibrated with the Raman peak of Silicon SCs at 520.7 cm^{-1} .

CL spectra were collected with an optical spectrometer (model iHR 320, Horiba Jobin Yvon, Japan), which was attached to the SEM instrument (model Gemini G300, Carl Zeiss, Germany). XPS spectra were measured on a ThermoFisher Scientific ESCALAB 250X system, using a monochromatic $\text{Al K}\alpha$ source. The binding energy (BE) of the XPS was calibrated with respect to the pure bulk Au 4f_{7/2} (BE = 84.0

eV) and Cu 2p_{3/2} (BE = 932.7 eV) lines. The BE was referenced to the Fermi level (E_f) calibrated by using pure bulk Ni as $E_f = 0$ eV. XPS spectra were calibrated with C 1s peak from the sample and set to BE = 284.6 eV.

3. RESULTS AND DISCUSSIONS

Figure 1 shows the XRD patterns of the as-synthesized solvent by using the starting materials Sr_3N_2 and hBN powder. As can

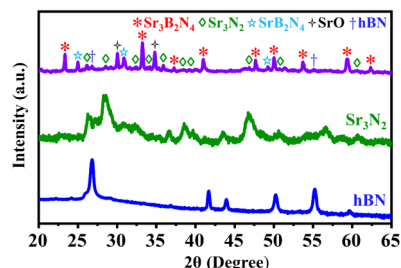
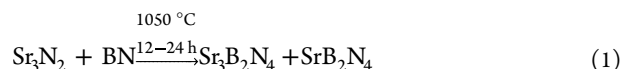


Figure 1. XRD patterns of the solvent and starting materials Sr_3N_2 and hBN. The major phase of the solvent was identified as $\text{Sr}_3\text{B}_2\text{N}_4$.

be seen, the major XRD peaks of the solvent can be identified as $\text{Sr}_3\text{B}_2\text{N}_4$ (JCPDF No. 49-1479), with some remaining feedstocks of hBN and Sr_3N_2 , as well as SrB_2N_4 and SrO phases. The presence of SrO is likely due to the residual oxygen in the tube furnace during high temperature annealing. Thus, the main transformation was concluded following eq1:



The typical T - P profiles for HPHT growth of hBN SCs are given in Figure 2a. The pressure was first ramped to 4.5 GPa within 2.5 h, and then the temperature was increased to 1500 $^\circ\text{C}$ and maintained for 15–20 h. Figure 2b depicts the sample

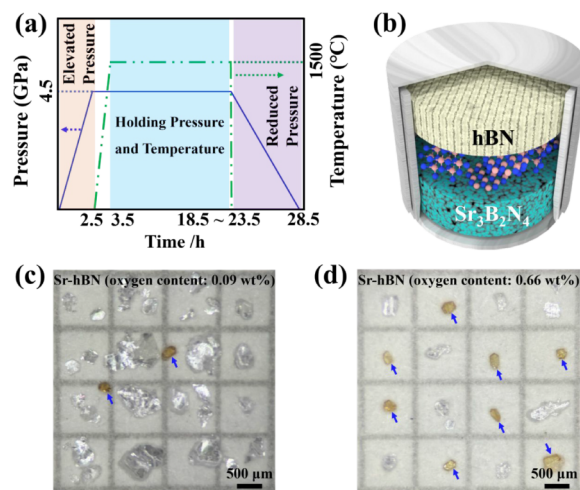


Figure 2. hBN SCs synthesized by the HPHT method. (a) Pressure and temperature profiles for the HPHT synthesis of hBN SCs. (b) Assembly of the high-pressure cell for the HPHT experiments. Cell size varies when using a small-sized chamber or a large-sized chamber, while the assembly structures remained similar. (c) and (d) Photographs showing the recovered hBN and cBN crystals as the main products from a single synthesis using hBN sources with oxygen contents of 0.09 and 0.66 wt %, respectively. Arrows indicate the cBN particles. A large-sized chamber was used for the growth of (c) and (d).

arrangement within the Mo capsule, for which the bilayer cylindrical structure ensures an effective sealing of the precursor. Figure 2c,d shows photographs of the obtained BN SCs grown out of the hBN sources with oxygen contents of 0.09 and 0.66 wt %, respectively. Both hBN and cubic BN (cBN) SCs precipitated simultaneously in the growth chamber. We found that the lower oxygen content in the hBN source (0.09 wt %) was beneficial for getting colorless and transparent plate-like-shaped hBN SCs with smooth surfaces as the major product. Such hBN SCs also show shining reflectance and relatively large size up to ~ 1.2 mm. In contrast, higher oxygen content (0.66 wt %) in the hBN source led to the production of smaller-sized hBN SCs with evidently lower yield; instead, the yield of cBN crystals increased (Figure 2c,d). Such a dependence of the hBN SCs yield on the oxygen content was essentially consistent with the Ba-based²² and Li-based systems.²⁵ Additionally, our studies also reveal comparable yield and crystal size by using the Sr-based solvent, in comparison to using the Ba-based solvent.

Figure 3a shows the XRD patterns of the hBN SCs grown in the present work. The XRD pattern of the hBN SCs from the National Institute of Materials Science Japan (NIMS-Ba-BN,

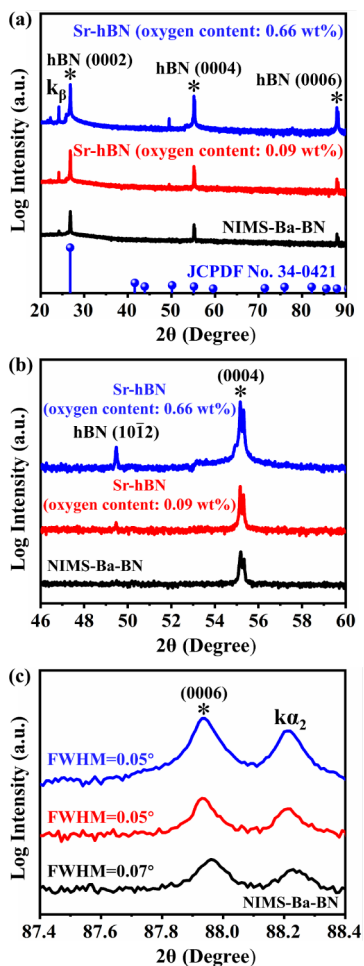


Figure 3. XRD patterns of hBN SCs from the HPHT method. (a) XRD profiles of the hBN SCs grown out of the source with 0.09 and 0.66 wt % oxygen content and the hBN SCs of Ba-based system from NIMS. The known crystallographic planes of hBN were labeled above the corresponding peaks. Enlarged view of the XRD patterns in the range of (b) 46° – 60° and (c) 87.4° – 88.4° .

batch No. M1012) is also shown for comparison. All samples exhibit the three most prominent XRD peaks, corresponding to the (0002), (0004), and (0006) reflections of hBN (JCPDF No. 34-0421).²⁶ A small but sharp peak around 50° associated with the hBN (10T2) reflection was observed in our hBN SCs, Figure 3b, which may arise from individual tilt-placed hBN SCs during the XRD measurement. In contrast to the Mg- and Na-based systems, where the rhombohedral BN (rBN) or Bernal phase BN (bBN) were frequently observed,^{20,21} the rBN or bBN phase was not detected in our samples (akin to the NIMS-Ba-BN samples). As shown in Figure 3c, the (0006) peak for our hBN SCs displays well-defined Gaussian line-shape with fwhm $\sim 0.05^{\circ}$, which is significantly narrower than that of the Mg-based system (fwhm $\sim 0.15^{\circ}$)²¹ and comparable to that of the Ba-based system (fwhm $\sim 0.07^{\circ}$, Figure 3c). Such a sharp XRD peak signals an excellent crystalline quality for our hBN SCs grown out of the Sr-based solvent.

To further characterize these crystals, we acquired Raman spectra at randomly chosen positions on the synthesized hBN SCs. As depicted in Figure 4, both samples (hBN SCs grown

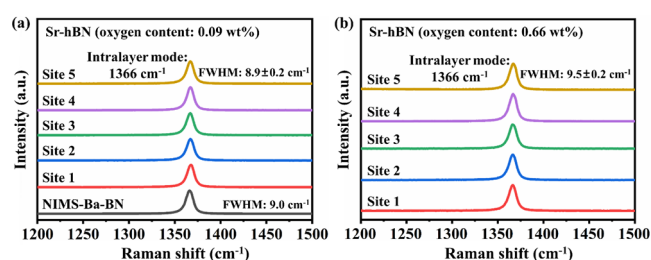


Figure 4. Raman spectrum of the hBN SCs synthesized from hBN sources with oxygen content of (a) 0.09 and (b) 0.66 wt %. The NIMS sample was also measured for comparison as shown in lower part of (a).

from the hBN source with oxygen content of 0.09 or 0.66 wt %) display the expected hBN intralayer E_{2g} vibrational mode, centered at 1366 cm^{-1} , with excellent uniformity across the samples. The variations in the peak position and the fwhm were within the instrument resolution over a range of approximately 0.7 mm. As shown in Figure 4a,b, upon reducing the oxygen content in the hBN sources, the fwhm of Raman peak indeed decreases from 9.5 cm^{-1} (0.66 wt %) to 8.9 cm^{-1} (0.09 wt %), which could be attributed to reduced density of oxygen-related defects. Thus, a better crystal quality was achieved for the hBN SCs using a precursor with low oxygen content. As shown in Figure 4a, the fwhm of the Raman spectra for our hBN SCs was comparable to that of Ba-based system from NIMS, suggesting similar quality of the SCs grown from these two different solvents.

Figure 5a–d shows typical room-temperature CL spectra of the hBN SCs. We performed CL measurements on multiple points to check the homogeneity. As shown in Figure 5a,b, the CL spectra of the hBN SCs grown from the lower oxygen content source (0.09 wt %) share similar characteristics with that of hBN SCs from NIMS-Ba-BN. Specifically, we observed an intense peak in the CL spectrum around 5.76 eV, corresponding to the intrinsic longitudinal optical (LO) phonon-related emission.²⁷ In addition, there exists two subpeaks at 5.58 and 5.32 eV, which were attributed to the stacking fault-related emission (the D series lines).²⁸ Although the stacking fault-mediated emission competes with the intrinsic phonon-assisted recombination, the observation of

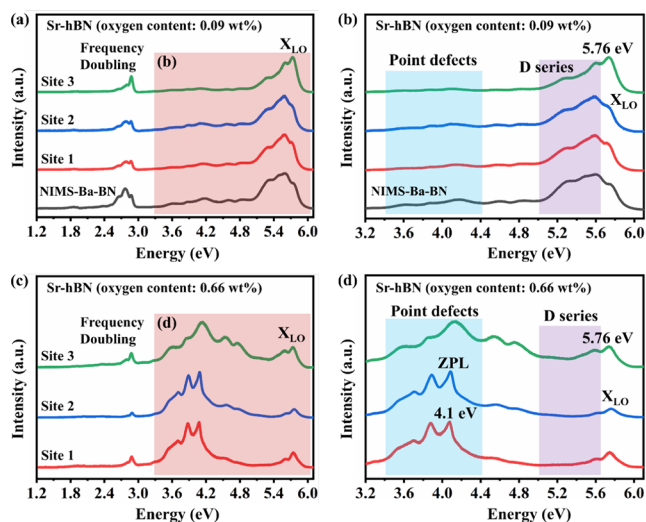


Figure 5. CL of the hBN SCs synthesized from the hBN source with oxygen contents of (a) 0.09 wt % and (c) 0.66 wt %. (b) and (d) Magnified regions between 3.2 and 6.1 eV. The NIMS sample was also measured for comparison as shown in the lower part of (a) and (b).

intensive phonon-assisted peaks at this region signals the high quality of the hBN SCs. In addition to the peaks around 5.76 eV, we also observed the frequency doubling peaks at around 2.88 eV. Typical point defect-related peaks around 2.05 eV²⁹ and 4.1 eV³⁰ were not detected, again verifying the high quality of our crystals. On the contrary, for the hBN SCs grown from the high-oxygen content sources (0.66 wt %), the intrinsic phonon-assisted peak around 5.76 eV was relatively weak, while the point defect-related emission peaks around 4.1 eV become much stronger (as shown in Figure 5c,d). Slight site-to-site variations were also observed for these bands. The observation of the peaks around ~4.1 eV indicated that the incorporation of oxygen into the hBN precursors directly influences the final properties of hBN SCs.^{22,28} This observation was also consistent with previous report.¹⁵ It is noted that the presence of SrO in Sr₃B₂N₄ solvent seems to show no evident effect on the CL properties and the crystalline quality of the final hBN SCs, although it might occupy a certain percentage in the solvent (as judged from the XRD peak intensity). This might be attributed to high melting point of SrO (~2430 °C), which is significantly higher than that of BaO (~1920 °C), ensuring its stability and possibly preventing its involvement in chemical transformations during hBN SC growth.

To further check the purity/chemical composition of the resultant crystals, we performed XPS measurements on the hBN SCs grown from the hBN source with lower oxygen content (0.09 wt %). Figure 6a displays the wide-scan XPS spectra, featuring prominent peaks assigned to B 1s and N 1s, along with minor peaks associated with C 1s, O 1s, and Mo 3d, respectively. The observed Mo 3d signal could be ascribed to some residual Mo particles. The B 1s peak at 190.5 eV (as shown in Figure 6b) and N 1s peak at 398.0 eV (as shown in Figure 6c) were in good agreement with previously reported values in literature.³¹ Both B and N related peaks can be well fitted by using a single Gauss–Lorentz function (Figure 6b,c), and the B/N ratio was confirmed to be 1:1. The absence of C–N or C–B bonding states, as well as the Sr peaks, further elaborates the high purity of the obtained hBN SCs.³²

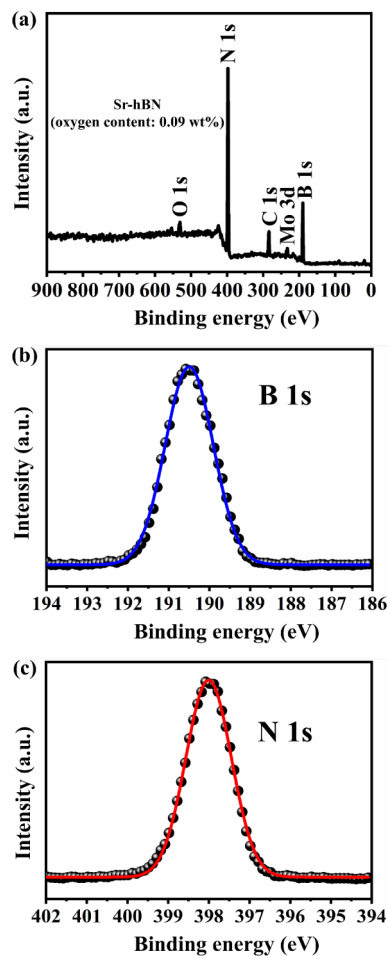


Figure 6. XPS of the hBN SCs synthesized from the hBN source with oxygen content of 0.09 wt %. (a) XPS wide scan of the hBN SCs. High-resolution XPS spectra were measured for (b) the B 1s and (c) the N 1s peaks.

4. SUMMARY

In summary, we demonstrate that Sr₃B₂N₄ is an effective solvent for the HPHT growth of high-quality hBN SCs with in-plane dimensions up to 1.2 mm, which was comparable to those grown from the Ba₃B₂N₄ solvent. The XPS spectra revealed a B/N ratio of 1:1 without the detection of C–N or C–B bonds, and multiple characterizations using XRD, Raman, and CL spectra confirm a superior crystalline quality for these hBN SCs grown out of the Sr₃B₂N₄ solvent. We also verified the viability of this route in both small-sized and large-sized chambers, paving the way for large-scale growth of high-quality hBN SCs. Consequently, we have established an alternative, low-cost route for the large-scale synthesis of high-quality hBN SCs under HPHT conditions.

AUTHOR INFORMATION

Corresponding Authors

Neng Wan – Key Laboratory of MEMS of Ministry of Education, College of Integrated Circuits, Southeast University, Nanjing 210096, China; orcid.org/0000-0003-3120-0307; Email: wn@seu.edu.cn

Jinguang Cheng – Beijing National Laboratory for Condensed Matter Physics and Institute of Physics, Chinese Academy of Science, Beijing 100190, China; School of Physical Sciences, University of Chinese Academy of Science, Beijing 100190,

China; orcid.org/0000-0002-4969-1960;
Email: jgcheng@iphys.ac.cn

Authors

Ming Tian – Key Laboratory of MEMS of Ministry of Education, College of Integrated Circuits, Southeast University, Nanjing 210096, China; Beijing National Laboratory for Condensed Matter Physics and Institute of Physics, Chinese Academy of Science, Beijing 100190, China

Ning-Ning Wang – Beijing National Laboratory for Condensed Matter Physics and Institute of Physics, Chinese Academy of Science, Beijing 100190, China; School of Physical Sciences, University of Chinese Academy of Science, Beijing 100190, China; orcid.org/0000-0002-2820-4094

Gang Wang – Beijing National Laboratory for Condensed Matter Physics and Institute of Physics, Chinese Academy of Science, Beijing 100190, China; School of Physical Sciences, University of Chinese Academy of Science, Beijing 100190, China

Md Al Shahriar Akash – Key Laboratory of MEMS of Ministry of Education, College of Integrated Circuits, Southeast University, Nanjing 210096, China

Hui Shi – Key Laboratory of MEMS of Ministry of Education, College of Integrated Circuits, Southeast University, Nanjing 210096, China

Junpeng Shu – Key Laboratory of MEMS of Ministry of Education, College of Integrated Circuits, Southeast University, Nanjing 210096, China

Ruowang Chen – Key Laboratory of MEMS of Ministry of Education, College of Integrated Circuits, Southeast University, Nanjing 210096, China

Nadia Afzal – Key Laboratory of MEMS of Ministry of Education, College of Integrated Circuits, Southeast University, Nanjing 210096, China

Zhenning Hu – Key Laboratory of MEMS of Ministry of Education, College of Integrated Circuits, Southeast University, Nanjing 210096, China

Shun-Shun Yang – College of Physical, Nanjing University of Aeronautics and Astronautics, Key Laboratory of Aerospace Information Materials and Physics (NUAA), MIIT, Nanjing 210016, China; orcid.org/0000-0002-7488-1125

Linglong Zhang – College of Physical, Nanjing University of Aeronautics and Astronautics, Key Laboratory of Aerospace Information Materials and Physics (NUAA), MIIT, Nanjing 210016, China

Yu Zhang – School of Materials Science and Engineering, Materials Genome Institute, Shanghai University, Shanghai 200444, China

Juanjuan Xing – School of Materials Science and Engineering, Materials Genome Institute, Shanghai University, Shanghai 200444, China

Kenji Watanabe – National Institute for Materials Science (NIMS), Ibaraki 305-0047, Japan; orcid.org/0000-0003-3701-8119

Takashi Taniguchi – National Institute for Materials Science (NIMS), Ibaraki 305-0047, Japan; orcid.org/0000-0002-1467-3105

Complete contact information is available at:
<https://pubs.acs.org/10.1021/acs.cgd.4c01079>

Author Contributions

[∇]M.T. and N.-N.W. contributed equally to this work.

Notes

The authors declare no competing financial interest.

ACKNOWLEDGMENTS

The authors thank Dr Yuanbo Zhang at Fudan University for the initiative of this work. This work was supported by the National Natural Science Foundation of China (Grant Nos. 12025408, 61504030, 61370042, and 61006011) National Key Research and Development Program of China (Grant No. 2023YFA1406100), and Postgraduate Research & Practice Innovation program of Jiangsu province KYCX22_0228. The first author acknowledges the China Scholarship Council (CSC).

REFERENCES

- (1) Cao, J.; Tian, M.; Zhang, S.; Hu, W.; Wan, N.; Lin, T. Carbon-related defect control of bulk hBN single crystals growth by atmospheric-pressure metal-flux-based fusion synthesis. *J. Mater. Sci.* **2022**, *57*, 14668–14680.
- (2) Dean, C. R.; Young, A. F.; Meric, I.; Lee, C.; Wang, L.; Sorgenfrei, S.; Watanabe, K.; Taniguchi, T.; Kim, P.; Shepard, K. L.; Hone, J. Boron nitride substrates for high-quality graphene electronics. *Nat. Nanotechnol.* **2010**, *5*, 722–726.
- (3) Xi, X. X.; Wang, Z. F.; Zhao, W. W.; Park, J. H.; Law, K. T.; Berger, H.; Forro, L.; Shan, J.; Mak, K. F. Ising pairing in superconducting NbSe₂ atomic layers. *Nat. Phys.* **2016**, *12*, 139–143.
- (4) Petrone, N.; Chari, T.; Meric, I.; Wang, L.; Shepard, K. L.; Hone, J. Flexible Graphene Field-Effect Transistors Encapsulated in Hexagonal Boron Nitride. *ACS Nano* **2015**, *9*, 8953–8959.
- (5) Wang, X.; Hossain, M.; Wei, Z.; Xie, L. Growth of two-dimensional materials on hexagonal boron nitride (h-BN). *Nanotechnology* **2019**, *30*, 034003.
- (6) Watanabe, K.; Taniguchi, T. Hexagonal Boron Nitride as a New Ultraviolet Luminescent Material and Its Application. *Int. J. Appl. Ceram. Technol.* **2011**, *8*, 977–989.
- (7) Watanabe, K.; Taniguchi, T.; Niiyama, T.; Miya, K.; Taniguchi, M. Far-ultraviolet plane-emission handheld device based on hexagonal boron nitride. *Nat. Photonics* **2009**, *3*, 591–594.
- (8) Ahmed, K.; Dahal, R.; Weltz, A.; Lu, J.-Q.; Danon, Y.; Bhat, I. B. Growth of hexagonal boron nitride on (111) Si for deep UV photonics and thermal neutron detection. *Appl. Phys. Lett.* **2016**, *109*, 113501.
- (9) Janzen, E.; Schutte, H.; Plo, J.; Rousseau, A.; Michel, T.; Desrat, W.; Valvin, P.; Jacques, V.; Cassabois, G.; Gil, B.; et al. Boron and Nitrogen Isotope Effects on Hexagonal Boron Nitride Properties. *Adv. Mater.* **2024**, *36*, 2306033.
- (10) Caldwell, J. D.; Kretinin, A. V.; Chen, Y.; Giannini, V.; Fogler, M. M.; Francescato, Y.; Ellis, C. T.; Tischler, J. G.; Woods, C. R.; Giles, A. J.; et al. Sub-diffractive volume-confined polaritons in the natural hyperbolic material hexagonal boron nitride. *Nat. Commun.* **2014**, *5*, 5221.
- (11) Wang, L.; Xu, X. Z.; Zhang, L. N.; Qiao, R. X.; Wu, M. H.; Wang, Z. C.; Zhang, S.; Liang, J.; Zhang, Z. H.; Zhang, Z. B.; Chen, W.; Xie, X. D.; Zong, J. Y.; Shan, Y. W.; Guo, Y.; Willinger, M.; Wu, H.; Li, Q. Y.; Wang, W. L.; Gao, P.; Wu, S. W.; Zhang, Y.; Jiang, Y.; Yu, D. P.; Wang, E. G.; Bai, X. D.; Wang, Z. J.; Ding, F.; Liu, K. H. Epitaxial growth of a 100-square-centimetre single-crystal hexagonal boron nitride monolayer on copper. *Nature* **2019**, *570*, 91–95.
- (12) Ohta, J.; Fujioka, H. Sputter synthesis of wafer-scale hexagonal boron nitride films via interface segregation. *APL Mater.* **2017**, *5*, 076107.
- (13) Laleyan, D. A.; Mengle, K.; Zhao, S.; Wang, Y.; Kioupakis, E.; Mi, Z. Effect of growth temperature on the structural and optical properties of few-layer hexagonal boron nitride by molecular beam epitaxy. *Opt. Express* **2018**, *26*, 23031–23039.

- (14) Li, Y.; Garnier, V.; Steyer, P.; Journet, C.; Toury, B. Millimeter-Scale Hexagonal Boron Nitride Single Crystals for Nanosheet Generation. *ACS Appl. Nano Mater.* **2020**, *3*, 1508–1515.
- (15) Kubota, Y.; Watanabe, K.; Tsuda, O.; Taniguchi, T. Deep Ultraviolet Light-Emitting Hexagonal Boron Nitride Synthesized at Atmospheric Pressure. *Science* **2007**, *317*, 932–934.
- (16) Kubota, Y.; Watanabe, K.; Tsuda, O.; Taniguchi, T. Hexagonal Boron Nitride Single Crystal Growth at Atmospheric Pressure Using Ni–Cr Solvent. *Chem. Mater.* **2008**, *20*, 1661–1663.
- (17) Onodera, M.; Taniguchi, T.; Watanabe, K.; Isayama, M.; Masubuchi, S.; Moriya, R.; Machida, T. Hexagonal Boron Nitride Synthesized at Atmospheric Pressure Using Metal Alloy Solvents: Evaluation as a Substrate for 2D Materials. *Nano Lett.* **2020**, *20*, 735–740.
- (18) Liu, S.; He, R.; Ye, Z. P.; Du, X. Z.; Lin, J. Y.; Jiang, H. X.; Liu, B.; Edgar, J. H. Large Scale Growth of High-Quality Hexagonal Boron Nitride Crystals at Atmospheric Pressure from a Fe–Cr Flux. *Cryst. Growth Des.* **2017**, *17*, 4932–4935.
- (19) Zhang, N. F.; Yang, N. J.; Wang, W. J.; Zhong, X.; Chen, X. L. Growth of hexagonal boron nitride crystals at atmospheric pressure from Cu–Cr flux. *J. Cryst. Growth* **2021**, *562*, 126074.
- (20) Yano, M.; Okamoto, M.; Yap, Y. K.; Yoshimura, M.; Mori, Y.; Sasaki, T. Growth of nitride crystals, BN, AlN and GaN by using a Na flux. *Diamond Relat. Mater.* **2000**, *9*, 512–515.
- (21) Zhigadlo, N. Crystal growth of hexagonal boron nitride (hBN) from Mg–B–N solvent system under high pressure. *J. Cryst. Growth* **2014**, *402*, 308–311.
- (22) Taniguchi, T.; Watanabe, K. Synthesis of high-purity boron nitride single crystals under high pressure by using Ba–BN solvent. *J. Cryst. Growth* **2007**, *303*, 525–529.
- (23) Kubota, Y.; Watanabe, K.; Taniguchi, T. Synthesis of Cubic and Hexagonal Boron Nitrides by Using Ni Solvent under High Pressure. *J. Appl. Phys.* **2007**, *46*, 311–314.
- (24) Sun, F. P.; Hao, Z. R.; Liu, G. Z.; Wu, C. P.; Lu, S. Q.; Huang, S. R.; Liu, C.; Hong, Q. M.; Chen, X. H.; Cai, D. J.; Kang, J. Y. p-Type conductivity of hexagonal boron nitride as a dielectrically tunable monolayer: Modulation doping with magnesium. *Nanoscale* **2018**, *10*, 4361.
- (25) Taniguchi, T.; Yamaoka, S. Spontaneous nucleation of cubic boron nitride single crystal by temperature gradient method under high pressure. *J. Cryst. Growth* **2001**, *222*, 549–557.
- (26) Rousseau, A.; Moret, M.; Valvin, P.; Desrat, W.; Li, J. H.; Janzen, E.; Xue, L. J.; Edgar, J. H.; Cassabois, G.; Gil, B. Determination of the optical bandgap of the Bernal and rhombohedral boron nitride polymorphs. *Phys. Rev. Lett.* **2021**, *5*, 064602.
- (27) Cassabois, G.; Valvin, P.; Gil, B. Hexagonal boron nitride is an indirect bandgap semiconductor. *Nat. Photonics* **2016**, *10*, 262–266.
- (28) Vuong, T. Q. P.; Cassabois, G.; Valvin, P.; Ouerghi, A.; Chassagneux, Y.; Voisin, C.; Gil, B. Phonon-Photon Mapping in a Color Center in Hexagonal Boron Nitride. *Phys. Rev. Lett.* **2016**, *117*, 097402.
- (29) Koperski, M.; Vaclavkova, D.; Watanabe, K.; Taniguchi, T.; Novoselov, K. S.; Potemski, M. Midgap radiative centers in carbon-enriched hexagonal boron nitride. *Proc. Natl. Acad. Sci. U. S. A.* **2020**, *117*, 13214–13219.
- (30) Pelini, T.; Elias, C.; Page, R.; Xue, L.; Liu, S.; Li, J.; Edgar, J. H.; Dréau, A.; Jacques, V.; Valvin, P.; Gil, B.; Cassabois, G. Shallow and deep levels in carbon-doped hexagonal boron nitride crystals. *Phys. Rev. Mater.* **2019**, *3*, 094001.
- (31) Liu, S.; He, R.; Xue, L.; Li, J.; Liu, B.; Edgar, J. H. Single Crystal Growth of Millimeter-Sized Monoisotopic Hexagonal Boron Nitride. *Chem. Mater.* **2018**, *30*, 6222.
- (32) Ngamprapawat, S.; Nishimura, T.; Watanabe, K.; Taniguchi, T.; Nagashio, K. Current Injection into Single-Crystalline Carbon-Doped h-BN toward Electronic and Optoelectronic Applications. *ACS Appl. Mater. Interfaces* **2022**, *14*, 25731–25740.